Cell Reports
Physical Science

CellPress
OPEN ACCESS

Article

# Hybrid sulfurothioate-based electrolyte improving aesthetics, performance, and stability of transparent NIR-dye-sensitized solar cells

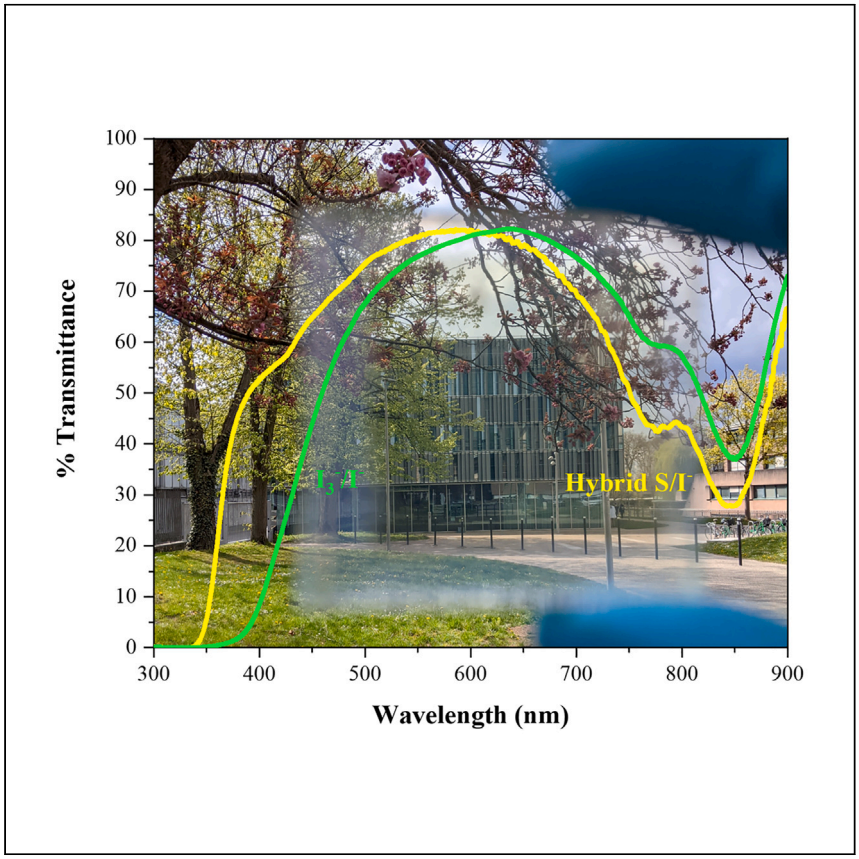


Transparent PV is a field aiming at PV integration for glass windows and, in this field, aesthetics can be as important as performance. Naim et al. report a colorless electrolyte that, when integrated into solar cells, affords notable technological improvement and matches the aesthetics of typical double glazing.

Waad Naim, Fionnuala Grifoni, Vijay Challuri, ..., Serge Pilard, Claudia Barolo, Frédéric Sauvage

frederic.sauvage@u-picardie.fr

## Highlights

The thioate-based electrolyte improves the aesthetics of NIR-DSSC for transparent PV

NIR-DSSC achieves an improved aesthetic level: AVT > 80%, CRI = 96, and 14% color purity

Hybrid thioate electrolyte improves performance and stability compared with standards

NIR-DSSC stability over 1,800 h is demonstrated

Naim et al., Cell Reports Physical Science 4, 101455
June 21, 2023 
https://doi.org/10.1016/j.xcrp.2023.101455

Cell Reports
Physical Science

CellPress
OPEN ACCESS

Article

# Hybrid sulfurothioate-based electrolyte improving aesthetics, performance, and stability of transparent NIR-dye-sensitized solar cells

Waad Naim,[1,6] Fionnuala Grifoni,[1,6] Vijay Challuri,[2] David Mathiron,[3] Sylvain Ceurstemont,[2] Pauline Chotard,[2] Thomas Alnasser,[1] Iva Dzeba,[1] Nadia Barbero,[4] Serge Pilard,[3] Claudia Barolo,[4,5] and Frédéric Sauvage[1,7,*]

## SUMMARY

**Enhancing performance, stability, and aesthetics is crucial for the development of transparent photovoltaics (TPV). In TPV, aesthetics are equally or even more important than performance because social acceptance requires maintaining aesthetics to a high level. In this work, we report a colorless hybrid electrolyte consisting of a thioate/iodide mixture. When integrated into wavelength-selective near-infrared-dye-sensitized solar cells (NIR-DSSCs), this electrolyte improves the power conversion efficiency (PCE) to up to 2.9% with a scattering layer and 2.1% in a transparent cell under AM1.5G conditions. It also reaches as high as 96% PCE retention over 1,800 h and confers an outstanding aesthetic level, up to 80% average visible transmittance (AVT), a color rendering index (CRI) of 96, and color purity as low as 14%, thus equaling the aesthetics of a double-glazed glass window.**

## INTRODUCTION

The mainstream in photovoltaic (PV) research is to approach the Shockley-Queisser (S-Q) limit through opaque technologies. Complementary to this conventional approach, semi-transparent to transparent absorbers are emerging concepts offering see-through features.[1] This new perception of PV panels creates a new value for PV integration while maximizing social acceptance. The end-member of this new PV stream is the transparent PV (TPV) technology, which is aesthetically the most deferential but also the most demanding in terms of materials development. Even though TPV has intrinsically lower performance than the conventional opaque counterpart, it can be imperceptibly deployed in our environment where passive glass windows are actually introduced. A theoretical power conversion efficiency (PCE) of 20.6% can be expected for a single-junction wavelength-selective TPV with an average visible transmittance (AVT) of 100%.[2] However, not all PV technologies can afford selective absorption of the near-infrared (NIR) region to reach high transparency. Indeed, the band structure, at the fate of conventional inorganic semiconductors, entails unselective photon absorption in which all photons with an energy greater than the bandgap value are absorbed. Therefore, achieving wavelength-selective absorption requires discrete orbital energy levels, which can only be achieved by molecular-based devices having a selective absorption fine-tuned outside the human eyes' photopic response (UV and/or NIR). Organic PV (OPV), luminescent solar cells (LSCs), quantum dots solar cells (QDSCs), and dye-sensitized solar cells (DSSCs) are the only technologies affording selective absorption. Lunt et al. were the first

[1]Laboratoire de Réactivité et Chimie des Solides, CNRS UMR7314, Université de Picardie Jules Verne, Hub de l'énergie, 15 Rue Baudelocque, 80039 Amiens Cedex, France

[2]G+LYTE SAS, 15 Rue Baudelocque, 80039 Amiens Cedex, France

[3]Analytical Platform, Université de Picardie Jules Verne, 33 Rue Saint-Leu, 80039 Amiens Cedex, France

[4]Department of Chemistry, NIS Interdepartmental and INSTM Reference Centre, University of Torino, Via Quarello 15, 10135 Torino, Italy

[5]ICxT Interdepartmental Centre, University of Torino, Lungo Dora Siena 100, 10153 Torino, Italy

[6]These authors contributed equally

[7]Lead contact

*Correspondence: frederic.sauvage@u-picardie.fr

https://doi.org/10.1016/j.xcrp.2023.101455

to propose a real selective TPV based on an organic planar heterojunction achieving 1.3% PCE with an AVT of 65%.[3] The introduction of new molecules organized into a bulk heterojunction has enhanced the performance (PCE = 4.0%) while maintaining a very good level of AVT (64%).[4] The American company Ubiquitous Energy recently announced a TPV production line and the achievement of 5.1% PCE and 51.5% AVT employing single-junction NIR-selective excitonic devices converting the range between 650 and 900 nm.[1] Nowadays, the highest AVT value is obtained for LSC technology (88.3%) thanks to its electrodeless technology. However, the efficiencies are still lagging, in the range of 1.5%.[1,5]

The optical rendering of DSSC technology is particularly advantageous because both coloration and transparency levels can be adjusted by the cell configuration and the involved chemistry. A green-colored see-through DSSC was reported with a PCE of 3.66% and a maximum transmittance value of 60% at 560 nm by a non-wavelength-selective co-sensitization approach.[6] Similarly, semi-transparent red DSSCs based on N719 dye were also recently proposed, reaching a maximum AVT of 44% and PCE up to 2.4%.[7,8] From a different approach, a photochromic semi-transparent DSSC was proposed by Demadrille et al. with an AVT of 59% in the dark and 27% under illumination, reaching a maximum PCE of 3.7%.[9] A certain amount of research has also been carried out to optimize large-area DSSC modules. Solaronix fabricated mini-modules based on the Ru-based dye N719 and a benzothiadiazole-based dye YKP-88.[10] The YKP-88 mini-module (23 $cm^2$) shows an aesthetic burgundy red tint with an AVT of 26% and a corresponding PCE of 8.7%. Recently, Di Carlo et al. optimized a semi-transparent dye-sensitized solar module of 400 $cm^2$, based on TTZ5 organic sensitizer, achieving 5.1% efficiency and transparency of 35.7%.[11] A more disruptive approach is the selective absorption of the NIR region in order to eliminate any perceptible coloration to human eyes. For this, the metal-free organic polymethine dyes are the most promising due to their high molar extinction coefficients (>140,000 $L.mol^{-1}cm^{-1}$) and red-shifted $S_0$-$S_1$ transition beyond 800 nm.[12,13] The concept of transparent NIR-selective DSSCs (NIR-DSSCs) was first reported based on the heptamethine cyanine dye (VG20-$C_{16}$), reaching an AVT of 65% in conjunction with the $I_3^-/I^-$ redox couple and a corresponding PCE of 2.0%.[14] Replacing the $I_3^-/I^-$ redox couple with $Co(bpy)_3^{3+/2+}$ enables a gain of 3% in AVT. To embrace such emerging TPV technologies for practical applications where architectural codes and social acceptance influence the domain, one needs to consider new figures of merit where optimizing PV performances and aesthetic quality is equally important. For the current NIR-DSSC technology, although high AVT values in the range of 70% have been reported, the final coloration defined by the CIE 1931 x,y coordinates and the color rendering index (CRI) was still in the yellowish-orange region. A new impetus is described in this work, where an outstanding level of transparency and neutral coloration are reported, thanks to a careful elimination of all factors contributing to coloration. This is achieved by the introduction of a new hybrid thioate/iodide-based electrolyte, minimization of dye aggregation, and inclusion of anti-reflecting coating, thanks to which we reached a remarkable aesthetic level (color neutrality, 80% AVT and CRI of 96), together with extensively enhancing the device stability without penalizing the device performances compared with the state-of-the-art $I_3^-/I^-$ redox couple.

## RESULTS AND DISCUSSION

### Synthesis and characterization

The conventional $I_3^-/I^-$ electrolyte (herein referred to as EI) has the main absorption band centered at 362 nm due to tri-iodide anions but exhibits a long absorption tail

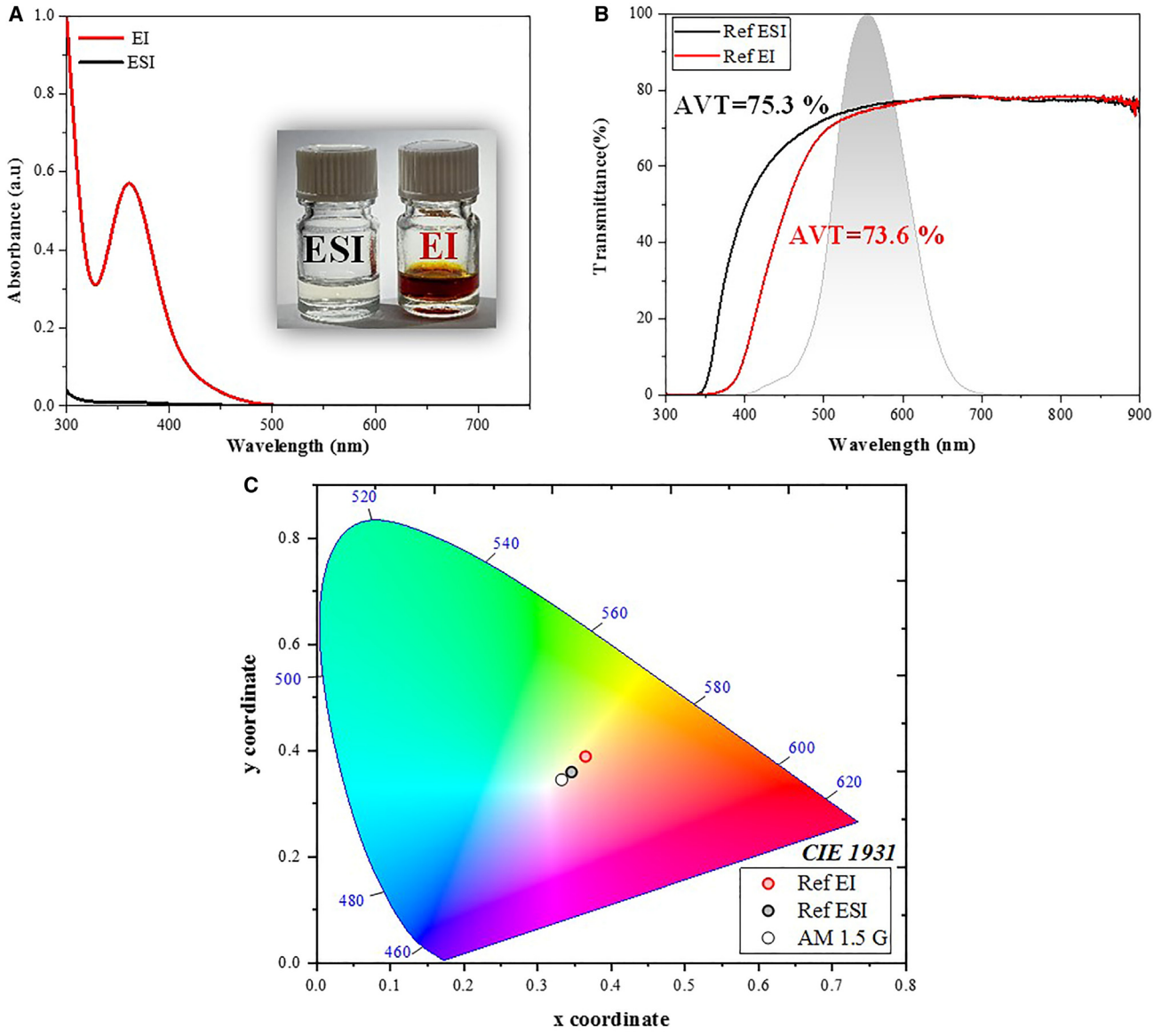


**Figure 1. Comparison between EI and hybrid ESI electrolyte**

(A) UV-visible absorption spectrum (pictures of the electrolytes shown in the inset).

(B) Total transmittance of the following structure: FTO glass/$TiO_2$/electrolyte/FTO glass compared with the photopic response of human eyes in gray. The electrolyte compositions are the optimized standards reported in the supplemental information.

(C) CIE 1931 chromaticity diagram. The white point represents AM1.5G coordinates used as a reference illuminant.

extending to the blue region where the humans' cones become sensitive (Figure 1A). For TPV application, replacing tri-iodide is one strategy to render the electrolyte colorless. In addition, it can maximize internal light utilization in combination with conventional visible dyes for standard DSSC. An elegant approach was proposed by Sun et al. where the authors introduced the notion of hybrid electrolyte, a tri-iodide free electrolyte, based on polysulfide/sulfide redox mediator ($S_5^{2-}/S^{2-}$) combined with iodide.[15] Inspired by this approach and herein introduced for the TPV application, we synthesized a tetramethylammonium S-methyl sulfurothioate, which, when incorporated with iodide, forms a new and transparent hybrid electrolyte (herein referred to as ESI). As a result, only a negligible absorption below 400 nm

is obtained without any contribution in the total visible range. The aesthetics metrics and evaluations are explained in Note S1 in the supplementary information.

The first intrinsic gain in aesthetics when using the hybrid ESI electrolyte has been quantified (i.e., without NIR-selective sensitizer). For this, the following structure was used: FTO glass/2-μm $TiO_2$/electrolyte/FTO glass. The AVT gain is ca. 2%, from 73.5% for EI electrolyte to 75.3% for the hybrid ESI electrolyte (Figure 1B). More importantly, the coloration with this new electrolyte composition is the most impactful, given the noticeable shift toward the white point reference AM1.5G in color coordinates from (x = 0.3646, y = 0.3877) to (x = 0.3455, y = 0.3585) (Figure 1C). Both the AVT gain and color coordinates shifting lead to an increase of CRI from 94 to 98.

High-resolution mass spectrometry (HRMS) analysis of ESI electrolyte, performed using electrospray ionization in the positive ion mode ($ESI^+$), confirmed that the main product is a tetramethylammonium S-methyl sulfurothioate salt, $CH_3$-S-$SO_3^-$ $TMA^+$, observed as a $TMA^+$ adduct (experimental *m/z* 275.1465, theoretical *m/z* 275.1463). The mass spectrometry (MS) analysis shows also that the electrolyte contains other minor products involving a core composed of a polysulfide chain with a number of sulfur atoms between two and four combined with $TMA^+$ cations (Note S2; Figure S1; Table S1). The presence of the sulfite group in the thioate is related to the synthesis performed under air conditions. We found that the synthetic atmosphere is a key parameter that affects the end product and the electrolyte performances. Indeed, by moving the synthesis from ambient conditions to a controlled argon inert atmosphere, the reaction gives only different polysulfide compounds and the resulting electrolyte does not perform as well (Table S2).[15] As described in the experimental part, a white precipitate is formed during the reaction and removed by filtration. This latter is composed of three zwitterionic molecules, HS-$SO_3^-$ $TMA^+$, $SO_4^{2-}$ $(TMA^+)_2$, and $^-$S-$SO_3^-$ $(TMA^+)_2$, observed as $TMA^+$ adducts at *m/z* 261.1298, 318.2415, and 334.2192, respectively. (Figure S2; Table S3). Both the transparency and the performance of the ESI electrolyte can be improved by purification on a reverse-phase column chromatography ($C_{18}$). It allows the retention of byproducts and thus the obtention of a more pure electrolyte solution as highlighted by MS (Figure S3).[16–18] The $^1H$ NMR spectrum showed signals with characteristic chemical shifts corresponding to the methyl groups of TMA (3.1 ppm) and of $CH_3$-S (1.9 ppm), confirming the tetramethylammonium S-methyl sulfurothioate $CH_3$-S-$SO_3^-$ $TMA^+$ structure (Figure S3). In such a complex chemical system, having numerous types of equilibrium reactions between different lengths of polysulfide chain, the type of solvent has an important role. For instance, the utilization of acetonitrile is paramount because it exhibits a relatively high dielectric constant (35.9) and a low donor number (14.1). These two characteristics are desirable to avoid polysulfide formation in the electrolyte over time, which may cause coloration uptake.[19–22] Cyclic voltammetry shows two successive oxidation peaks separated by around 200 mV. The first onset at 0.41 V vs. AgCl/Ag (ca. 0.63 V vs. NHE [normal hydrogen electrode]) is ascribed to the two-electron process thioate oxidation into the corresponding disulfide form (Figure S4). This value lies between the redox potential of di-iodide anion radical/iodide in acetonitrile ($E^{\circ\prime}(I_2^{-\cdot}/I^-)$ = 0.79V vs. NHE) and of tri-iodide/iodide redox couple ($E^{\circ\prime}(I_3^-/I^-)$ = 0.35 V vs. NHE).[23,24]

## Aesthetic evaluation

Sensitization conditions, photo-anode thickness, electrolyte composition, and anti-reflective coatings were carefully scrutinized parameters evaluated individually in addition to the impact on the AVT and color rendering characteristics of

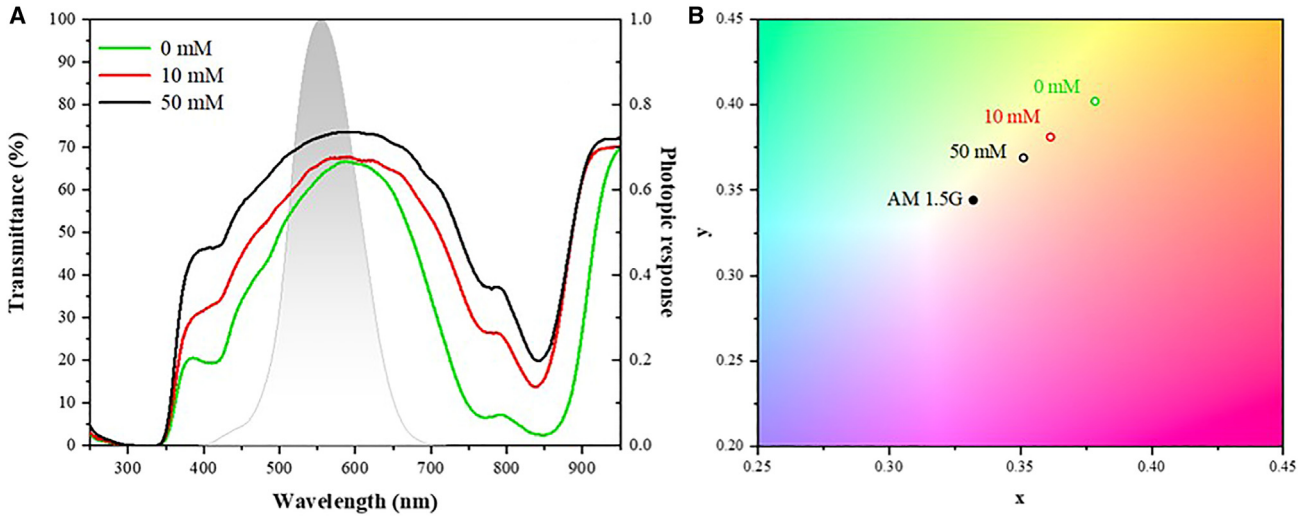


**Figure 2. Selective NIR-DSSC device containing inert electrolyte based on a 2-μm-thick $TiO_2$ photo-anode sensitized with VG20-$C_{16}$ dye**

The dye solution contains different CDCA concentrations (0 mM in green, 10 mM in red, and 50 mM in black).

(A) Evolution of the device transmittance including the human eye's photopic response as shaded gray curve.

(B) Evolution of the x,y coordinates in CIE 1931 color space diagram.

VG20-$C_{16}$-based selective NIR-DSSCs as a whole. The sensitization procedure is crucial because it preconditions the self-assembled monolayer (SAM) geometry and the molecular dye packing and therefore the dye-to-dye aggregation. The level of H-aggregation in the SAM is one critical aspect requiring careful attention since it will induce a broadening of the main $S_0$-$S_1$ transition in the NIR region, which can partially overlap within the human eye's photopic response, and thus is deleterious for the aesthetic rendering. It can also additionally induce new intermolecular absorptive contributions in the visible part.[14,25] To help in minimizing H-type aggregations, we introduced in our design a long lateral alkyl chain ($-C_{16}H_{33}$) on a polymethine core.[26] The introduction of a concentration of 50 mmol/L of chenodeoxycholic acid (CDCA) into the dye solution (100 μmol/L) corresponds with the optimized conditions to reach the greatest device performances.[14] As a consequence of this high CDCA to dye ratio, not only the dye loading is affected (Figure 2A) but also the H-aggregation level, which influences the device transparency and final coloration (Figure 2B).[27] For illustration, in the absence of CDCA, the transmission curve shows a minimum of 2.5% at 848 nm corresponding to the dye $S_0$-$S_1$ transition in contact with an inert electrolyte (i.e., no redox mediator). As a common feature of most polymethine dyes, an absorption shoulder is observable next to the $S_0$-$S_1$ transition at 765 nm. It stems from a combination of vibronic states within the molecule and aggregates excitation.[14] The absorption band at 410 nm corresponds to the upper-lying $S_0$-$S_n$ transitions. These bands do not overlay with the human eye's photopic response, thus making this dye an excellent candidate for TPV applications (Figure 2A). In this case, the device's AVT is 61%. With increasing CDCA ratio in solution, the $S_0$-$S_1$ transition gets narrowed (Figure S5) and the AVT is noticeably enhanced to 64% and 71% for 1:100 and 1:500 (dye:CDCA ratio), respectively. Less evident at first sight, dye aggregation influences not only the AVT but also the device tint (Figure 2B). This is shown in the calculated CIE 1931 x,y coordinates showing a continuous shift toward the white point coordinates. Consequently, one important highlight of this work is that the molecular dye aggregation is one key parameter influencing the CRI value, enhanced from 90 to 96 after optimization (Table 1).

**Table 1. Aesthetic characteristics of the selective NIR-DSSC based on VG20-$C_{16}$ for different CDCA concentration in full devices, including inert acetonitrile solvent**

| [CDCA] (mM) | AVT (%) | CRI | x,y CIE 1931 |
|---|---|---|---|
| 0 | 61 | 90.3 | x = 0.3786<br>y = 0.4018 |
| 10 | 64 | 93.8 | x = 0.3616<br>y = 0.3809 |
| 50 | 71 | 95.8 | x = 0.3513<br>y = 0.3687 |

The influence of the photo-anode thickness from 2 to 8 μm, bearing the chemisorbed sensitizer, is shown in Figure 3. An anti-reflective coating (ARC) based on a thin layer of $SiO_2$ nanoparticles was deposited by spin-coating on the external sides to minimize glass reflections.[28] The AVT value is correlated with the film's thickness. The AVT is decreasing from 76% for 2-μm thickness to 65% for 8 μm when the EI electrolyte is associated (Figure 3A). We reached a maximum AVT value of 80% for 2-μm-thick NIR-DSSC by replacing the standard electrolyte with the hybrid thioate/iodide electrolyte (Figure 3B). Such high AVT value reached with thin photo-anodes lies above the standard values reported for OPV and is akin to LSC technology.[5,29]

However, this gain of 4%, which is higher than the gain evaluated without the sensitizer, is only experienced for thin photo-anode thickness. Indeed, the AVT value tends to the same value of 65% for 8-μm thickness, as previously determined using EI electrolyte. This result stresses that the redox couple only influences the AVT when the $TiO_2$ photo-anode thickness is thinner than 6 μm. For thicker electrodes, it turns out that the AVT metric becomes governed by the optical characteristics of the nanocrystalline $TiO_2$ electrode. Note that, at this stage, no experimental evidence has been found that the level of dye aggregation is influenced by the photo-anode's thickness. The redox mediator influences the shape and position of the dye absorption band. This explains why an AVT difference of 4% is observed when the photo-anode is sensitized, whereas only 2% was obtained without the dye. This highlights the existence of a perceptible interaction between the dye and the redox mediator in the electrolyte in agreement with our previous work comparing $I_3^-/I^-$ redox couple and $Co(bpy)_3^{3+/2+}$-based electrolyte.[14] The ratio between the shoulder and the $S_0$-$S_1$ transition is higher in the case of ESI electrolyte (Figure S6). The absorption band maximum is also slightly blue shifted (i.e., 847 nm compared with 851 nm for the EI counterpart).

The AVT characteristic is important to ensure high visual comfort in seeing through the device. However, x,y chromaticity coordinates, CRI, the dominant wavelength, and color purity provide key information about how coloration is perceived looking at the device and how the latter modifies the color of an object. As for AVT, the $TiO_2$ thickness affects the color rendering. For the conventional EI electrolyte, the CIE x,y coordinates shift toward the white point by decreasing the electrode thickness from 8 to 2 μm. As a result, the CRI value is improved from 87.4, 89.0, 91.4, to 93.4 for the thinnest photo-anode (Table 2). A similar trend, but to a larger extent and with higher CRI values, is experienced for the hybrid ESI electrolyte (i.e., from 86.7, 90.2, 93.6, to 96.3 for 2-μm-thick $TiO_2$ photo-anode; Figure S7). The advantage of introducing the ESI electrolyte to improve the color rendering of the NIR-DSSC is highly noticeable for thicknesses where the photo-anode does not govern the final optical characteristics. Both dominant wavelength and color purity are intuitive quantities. They can be considered as an alternative to the numerical x,y

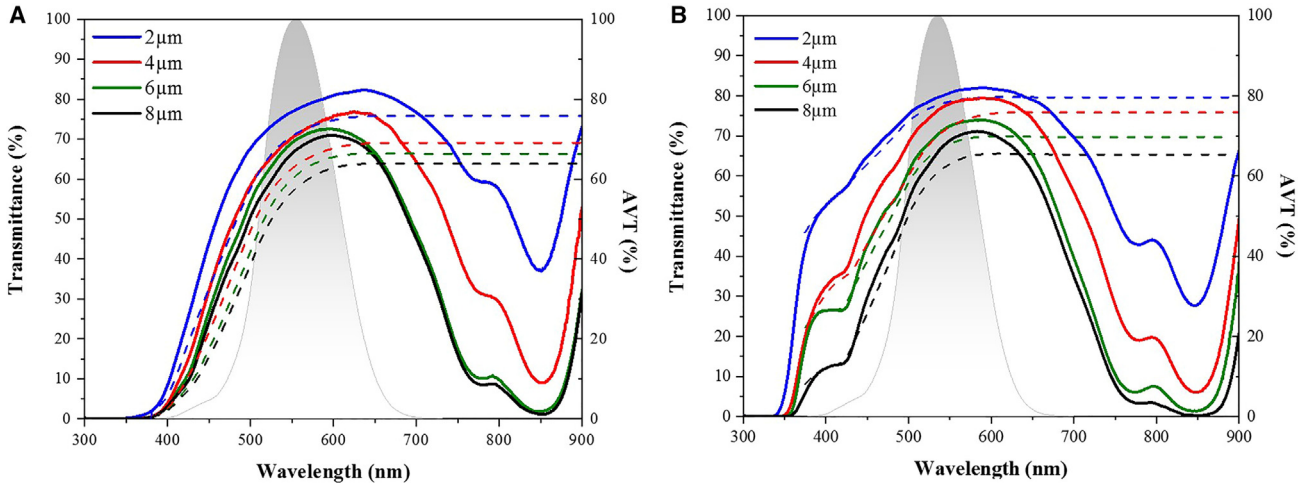


**Figure 3. Comparison of the total cell transmittance including the incremental evolution of AVT for NIR-DSSC devices using different $TiO_2$ thicknesses**

(A) $I_3^-/I^-$-based electrolyte (EI).

(B) Hybrid thioate/iodide electrolyte (ESI).

coordinates.[30] The dominant wavelength with EI electrolyte is 573 nm, corresponding to orange-yellow. It is 570 nm in the case of ESI electrolyte, corresponding to a slightly lighter yellow coloration, however, which may not be totally perceptible by human eyes (Figure 4). The difference in final perception originates from the color purity (color saturation) which is 0.31 (31%) in the case of EI electrolyte and only 0.14 (14%) for ESI electrolyte. This is one important advantage of this new electrolyte. It contributes to rendering the device significantly paler in coloration since the colorimetric position of the device's tint lies near to the white reference, thus rendering the photo-active part of the NIR-DSSC technology significantly less discernable. The evolution of the color purity is also determined for all thicknesses, highlighting once again how the color changes and becomes more saturated with thicker electrodes (Table 2).

### *PV characteristics and stability*

The PV characteristics were compared using the two electrolytes under AM1.5G conditions in the presence of a scattering layer. After optimization of $CH_3$-S-$SO_3^-$ $TMA^+$ and additives concentration (Table S4), a PCE of 2.4% ($V_{oc}$ = 359 mV, $J_{sc}$ = 11.2 mA/cm$^2$, FF = 58%) for ESI electrolyte is obtained compared with 2.6% for the reference EI electrolyte ($V_{oc}$ = 402 mV, $J_{sc}$ = 11.5 mA/cm$^2$, FF = 58%) (Figure 5A; Table 3). However, these performances can be further improved by introducing PV-grade G + Lyte ESI electrolyte leading to a PCE record of 2.9% ($V_{oc}$ = 363 mV, $J_{sc}$ = 12.8 mA/cm$^2$, FF = 57%). The corresponding external quantum efficiency (EQE) spectra of the champion devices with the integrated current are reported in Figure 5B. It shows higher EQE values for the purified ESI electrolyte in good agreement with the J-V curve. The main advantage of having a transparent electrolyte such ESI is to improve the dye conversion efficiency of the $S_0$-$S_n$ transitions at ca. 430 nm. The maximum EQE value reaches 64% at 850 nm, leading to an integrated current of 11.5 mA/cm$^2$.

In addition, this new electrolyte affords to enhance substantially the device stability. We reached as long as 1,800 h aging with an excellent PCE retention of 96% under shelf-life condition, and 1,000 h at 50°C/dark with a retention close to 80% using MPN-based ESI electrolyte (Figure S8). These are remarkable results given that

**Table 2. Aesthetic characteristics as a function of the photo-anode thickness for the complete NIR-DSSC for EI and ESI electrolyte**

| $TiO_2$ thickness (μm) | Electrolyte | AVT (%) | AVT with ARC (%) | CRI | Color purity (%) | x,y CIE 1931 |
|---|---|---|---|---|---|---|
| 2 | EI | 70 | 76 | 93.6 | 31 | x = 0.3743<br>y = 0.3970 |
| | ESI | 74 | 80 | 96.3 | 14 | x = 0.3484<br>y = 0.3653 |
| 4 | EI | 66 | 72 | 91.4 | 40 | x = 0.3886<br>y = 0.4128 |
| | ESI | 70 | 76 | 93.6 | 22 | x = 0.3593<br>y = 0.3816 |
| 6 | EI | 64 | 69 | 89.0 | 41 | x = 0.3823<br>y = 0.4152 |
| | ESI | 66 | 70 | 90.2 | 31 | x = 0.3698<br>y = 0.3992 |
| 8 | EI | 60 | 65 | 87.4 | 48 | x = 0.3979<br>y = 0.4279 |
| | ESI | 60 | 65 | 86.7 | 41 | x = 0.3848<br>y = 0.4206 |

cyanine dyes are regarded as poorly stable dyes and that their stability when incorporated in DSSC has never been demonstrated before. For comparison, under the same aging conditions, $T_{80}$ is only 280 h with EI electrolyte ($T_{80}$ refers to the time reaching 80% PCE retention). This result stresses the important role played by the redox mediator and its purity on the electrolyte.

Intensity-modulated photovoltage/photocurrent spectroscopies (IMVS/IMPS) show that the hybrid electrolyte influences neither the electron transport nor the electron lifetime (Figures S9A and S9B). It also has no influence on the distribution and energetics of the surface trap states in $TiO_2$ (Figure S9C).

To get a better insight into the role of this new thioate molecule on the dye regeneration, ps-pump probe transient absorption spectroscopy experiments have been carried out (Figure 6). The transient VG20-$C_{16}$ radical cation has a broad absorption contribution between 500 and 700 nm.[31] The exponential decay systematically requires two components to properly account for the decay, with an average half-time of $<\tau_{avg}>$ = 2.8 μs for EI electrolyte and $<\tau_{avg}>$ = 1.8 μs for ESI electrolyte (Figure 6B). This shows that the thioate-based hybrid electrolyte has a composition slightly advantageous for the dye regeneration. However, the dye regeneration kinetic is independent of the thioate concentration at a fixed concentration of iodide (Figure S10). This result highlights that the thioate species has no direct role in the dye regeneration but is rather an intermediate of the reaction. Indeed, the dye regeneration still proceeds through the di-iodide anion radical, where the thioate is an intermediate to produce a transient tri-iodide species. This herein-proposed mechanism is in agreement with Sun et al.'s proposition on polysulfide-based hybrid electrolyte.[15] The formation of transient tri-iodide species is supported by the fact that a similar electrocatalytic activity of platinum back-electrode was obtained compared with EI electrolyte, whereas platinum is acknowledged to be a poor catalyst for disulfide/thiolate redox reactions.[32]

More precisely, based on transient absorption results and the position of the redox potential for which the S-methyl sulfurothioate oxidation potential to disulfide lies between the two values of $I_2^{-\cdot}/I^-$ ($E°'(I_2^{-\cdot}/I^-)$ = 0.79 V vs. NHE) and $I_3^-/I^-$

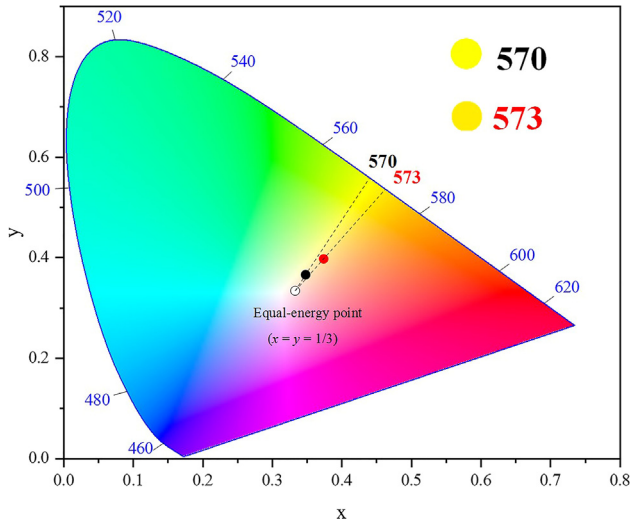


**Figure 4. CIE 1931 x and y coordinates calculated for the complete NIR-DSSC**
Using a 2-μm-thick $TiO_2$ electrode, EI electrolyte (red point) and ESI electrolyte (black point).

$(E^{\circ\prime}(I_3^-/I^-) = 0.35$ V vs. NHE),[23,24] the proposed mechanism to account for the VG20-$C_{16}$ dye regeneration is the following:

$$TiO_2|dye \xrightarrow{hv} TiO_2|dye^+ + e^-_{CB} \quad \text{(Equation 1)}$$

$$TiO_2|dye^+ + I^- \rightarrow TiO_2|(dye\cdots I) \quad \text{(Equation 2)}$$

$$TiO_2|(dye\cdots I) + I^- \rightarrow TiO_2(dye) + I_2^{-\cdot} \quad \text{(Equation 3)}$$

$$CH_3SSO_3^- + I_2^{-\cdot} \rightarrow \tfrac{1}{2}(CH_3SSO_3)_2 + 2I^- \quad \text{(Equation 4)}$$

$$\tfrac{1}{2}(CH_3SSO_3)_2 + 4I^- \rightarrow CH_3SSO_3^- + I_3^- + I^- \quad \text{(Equation 5)}$$

and in this mechanism, we assumed that reaction (4) is significantly faster than the di-iodide anion radical disproportionation, which has a rate constant in the range of ca. $2 \times 10^9$ $M^{-1}$ $s^{-1}$ in acetonitrile.[33] Given the rate constant of dye regeneration of $5.4 \times 10^5$ $s^{-1}$, the generated transient concentration of tri-iodide in the electrolyte remains sufficiently low to maintain the electrolyte colorless even under AM1.5G illumination.

The relationship between PCE, AVT, and light utilization efficiency (LUE) as a function of the photo-anode thickness for transparent devices (i.e., without scattering layer) is reported in Figure S11. The PCE is not inversely proportional to the AVT as is expected in non-wavelength-selective TPV. In the case of the NIR-DSSC, it reaches a maximum value for 6-μm-thickness films, i.e., 1.9% PCE at 69% AVT for EI and 2.1% PCE and 70% AVT for the optimized ESI electrolyte from G + Lyte (Voc = 356 mV, Jsc = 10.4 mA/cm$^2$, FF = 55%). Consequently, the LUE value reaches a maximum of 1.5% for the ESI electrolyte. The measurement of the photon balance validates the absence of factual errors in efficiency and optical measurements and therefore confirms the robustness of the reported values of T(λ), R(λ), and EQE (λ) for the NIR-DSSC device (Figure S12).

This work introduces a new transparent electrolyte for NIR-DSSC. It is based on a mixture of S-methyl sulfurothioate/iodide hybrid redox system in which the

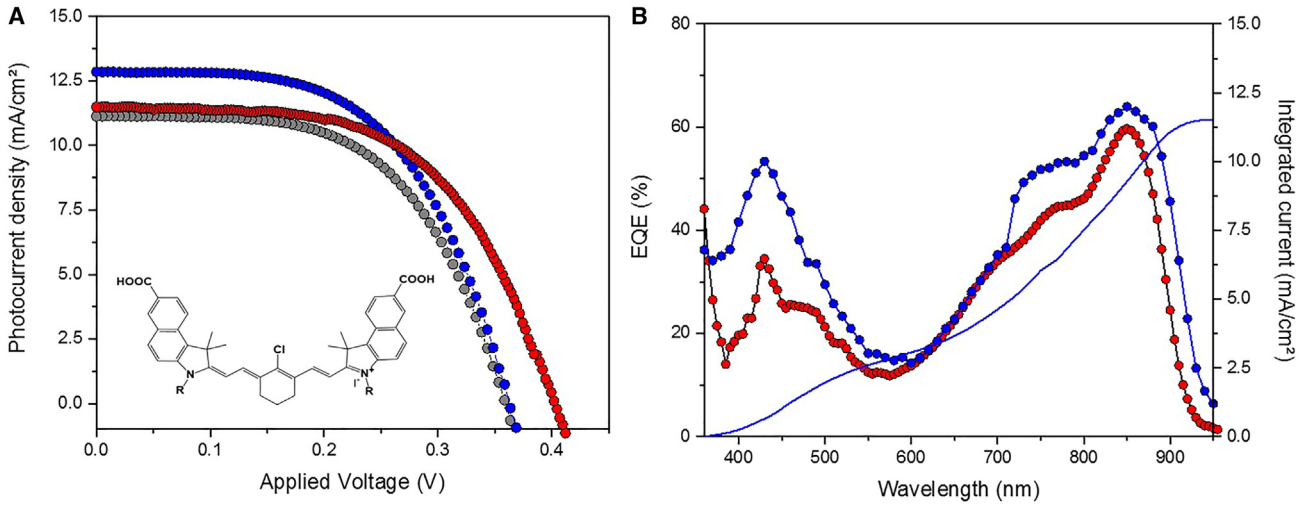


**Figure 5. NIR-DSSC cells characteristics**

(A) Evolution of the J–V curve under AM1.5G conditions of VG20-$C_{16}$ dye and photo-anode composed of 6-μm transparent layer sheltered by 5-μm-thick scattering layer with EI electrolyte (in red), ESI electrolyte (in black), and purified PV-grade ESI electrolyte (in blue). The general chemical structure of VG20-$C_{16}$ dye for which R correspond to $C_{16}H_{33}$ alkyl chain is reported in the inset.

(B) EQE curve obtained for EI electrolyte (in red) and purified PV-grade ESI electrolyte (in blue). The integrated current for the latter is reported for information.

peculiarity is to form transient tri-iodide in the electrolyte during dye regeneration at a sufficiently low concentration to maintain electrolyte transparency. This new transparent electrolyte affords improvement at once in all the key characteristics in the TPV triptych, namely (1) the aesthetic through an AVT reaching 80%, higher CRI of 96, and low color purity of only 14%; (2) higher PCE, reaching a maximum of 2.9% with a scattering layer and 2.1% without scattering layer; and (3) drastic enhancement of stability, reaching a PCE retention of 96% over 1,800 h of aging under shelf-life conditions and close to 80% PCE retention over 1,000 h of aging at 50°C/dark. All these key values are setting up a new state of the art in the field of wavelength-selective NIR-DSSC.

## EXPERIMENTAL PROCEDURES

### Resource availability

#### *Materials availability*

This study did not generate new unique materials.

#### *Lead contact*

Further information and requests for resources should be directed to and will be fulfilled by the lead contact, Frédéric Sauvage (frederic.sauvage@u-picardie.fr).

#### *Data and code availability*

All data from this study are available from the lead contact upon request.

### Reagents and materials

Tetramethylammonium hydroxide (25 wt % solution in water) and ammonium sulfide (17 wt % solution in water) were purchased from Alfa Aesar. Sulfur was purchased from Sigma-Aldrich (>99% purity metal basis). Dimethyl sulfoxide (DMSO), ethanol (EtOH), acetonitrile (ACN), chenodeoxycholic acid (CDCA), and lithium bis(trifluoromethane sulfonyl)imide (LiTFSI) were purchased from Sigma-Aldrich. Chemicals and solvents in this study were used as received without further purification. The colloidal $TiO_2$ paste DN-EP03 was purchased from Dyenamo.

**Table 3. Summary of cell characteristics with EI, ESI, and PV-grade ESI electrolyte under AM1.5G illumination (irradiance 0.92 sun for PV-grade ESI cell)**

| Electrolyte | $J_{SC}$ (mA/cm$^2$) | $V_{OC}$ (mV) | FF (%) | PCE (%) |
|---|---|---|---|---|
| EI | 11.5 | 402 | 58 | 2.6 |
| ESI | 11.2 | 359 | 58 | 2.4 |
| PV-grade ESI | 12.9 | 363 | 57 | 2.9 |

### Synthesis of tetramethylammonium S-methyl sulfurothioate

To prepare the tetramethylammonium sulfide, 44 mmol of tetramethyl ammonium is added to 22 mmol of ammonium sulfide; the mixture is stirred until the solution turns from yellow to colorless, and the water is then evaporated by rotary evaporation. The resulting white salt was dried at 50°C under vacuum. The S-methyl sulfurothioate with tetramethylammonium cation was synthesized by heating equivalent amounts (1.25 mmol) of sulfur and the lab-prepared tetramethylammonium sulfide in acetonitrile, then heated at 70°C for 3 h. The obtained solution is dark green, and it then turns transparent and colorless once it is left overnight at room temperature, in agreement with the literature.[15] The solution is then filtered and the filtrate kept for the preparation of the electrolyte.

### Electrolyte preparation

The optimized ESI electrolyte composition contains 1 mol/L 1,3-dimethylimidazolium iodide (DMII), 0.75 mol/L lithium iodide (LiI), and 0.02 mol/L tetramethylammonium S-methyl sulfurothioate ($CH_3$-S-$SO_3^-$ $TMA^+$). PV-grade electrolyte from G + Lyte is of the same composition. For comparison, the iodide-based electrolyte coded EI is composed of 1 mol/L DMII, 0.03 mol/L $I_2$, and 1 mol/L LiTFSI in acetonitrile as previously optimized.[14]

### Solar cell fabrication

The $TiO_2$ electrodes are deposited by screen printing yielding different thicknesses depending on the number of prints. The resulting films were post-annealed stepwise (325°C for 5 min, 375°C for 5 min, 450°C for 15 min, and 500°C for 15 min) to remove the porogen and terpineol solvent. BET analysis shows a surface area of 86.7 m$^2$/g and a mean pore size of 11 nm with a final porosity of 47% in the film. The electrodes were heated at 500°C in the air for 30 min before sensitization. For sensitization, the dye solution is composed of 0.1 mmol/L of VG20-$C_{16}$ and 50 mmol/L of chenodeoxycholic acid (CDCA) in a solvent mixture of DMSO/EtOH (1/9, v/v). The electrodes were immersed in the dye solution at 4°C for ca. 20 h. The combination of low sensitization temperature, highly diluted dye solution, and high concentration of CDCA avoids excessive formation of H-type and J-type aggregated dyes in the SAM.[14] The working electrode and the thermally deposited Pt-based counter-electrode were assembled using a thermoplastic 25-μm-thick Surlyn ring (DuPont, USA). Low-loading platinum (<0.6 wt %) counter-electrode was prepared by screen printing to yield a perfectly transparent electrode while displaying the required electro-activity, not to penalize efficiency. It reduces the AVT by ca. 4% while not modifying color perception. Pt-free counter-electrode was used for aesthetic evaluation of the photo-anode and electrolyte parameters. The electrolyte is inserted into the device by vacuum backfilling using a pre-drilled hole formed by sandblasting into the counter-electrode. The hole was sealed with a Surlyn sheet and a thin glass cover by heating. All PV characteristics and stability assessment were performed on black masked devices with 0.16-cm$^2$ aperture area. The dataset was reproduced. A deviation of less than 0.1% in device PCE are typically achieved in the lab.

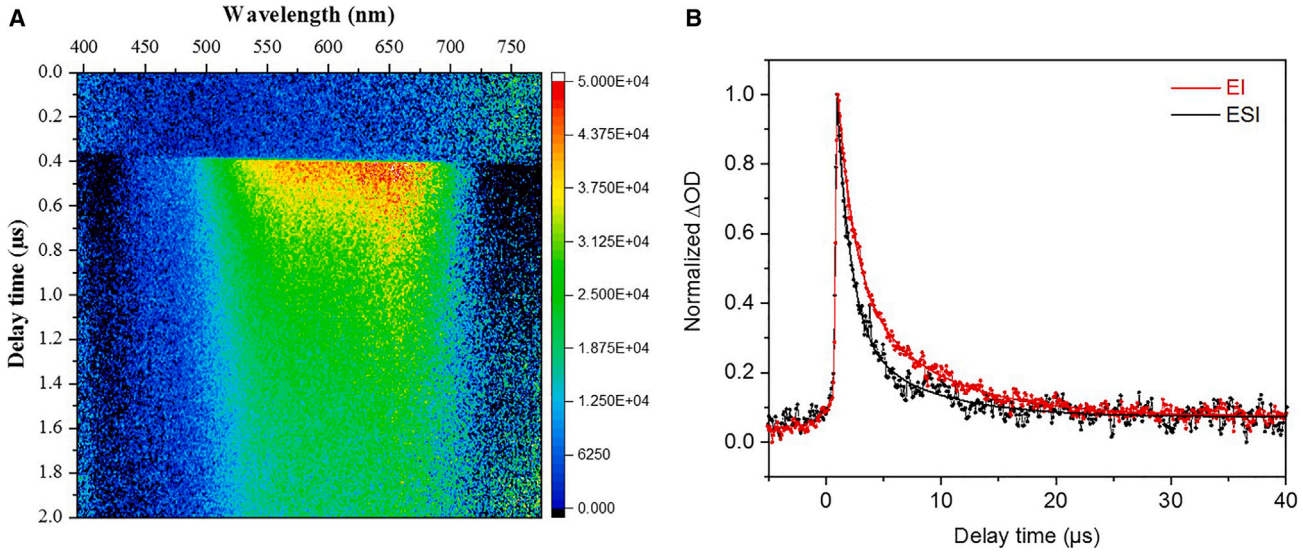


**Figure 6. Transient absorption measurements**

(A) Streak image of the time-resolved transient absorption spectrum corresponding to the dye regeneration of VG20-$C_{16}$ in NIR-DSSC in association with the ESI electrolyte. The black area corresponds to the dye ground-state bleaching.

(B) Comparison of transient absorption decay at 650 nm for EI electrolyte (in red) and ESI electrolyte (in black).

## SUPPLEMENTAL INFORMATION

Supplemental information can be found online at https://doi.org/10.1016/j.xcrp.2023.101455.

## ACKNOWLEDGMENTS

W.N. and F.S. wish to thank the Agence National de la Recherche (ANR) VISION-NIR program under grant agreement no. ANR-17-CE05-0037 for financial support. F.G., T.A., N.B., C.B., and F.S. acknowledge the IMPRESSIVE project, which received funding from the European Union's grant agreement no. 826013. The authors thank Prof. A. Di Carlo, Dr. F. Matteocci, and Dr. D. Rossi from University Tor Vegata for fruitful discussion on AVT and CRI assessment; Prof. S. Haacke from Université de Strasbourg and Dr. Y. Smortsova from Université de Lille for helpful comments and fruitful discussions about TAS experiments and results; and Dr. Fabrice Odobel (CEISAM, CNRS) and Dr. Matteo Bonomo (UNITO) for fruitful discussions.

## AUTHOR CONTRIBUTIONS

Conceptualization, W.N., F.G., and F.S.; investigation, F.G., W.N., D.M., V.C., S.P., S.C., and P.C.; synthesis – dye, N.B. and C.B.; writing – original draft, W.N. and F.G., writing – review & editing, W.N., F.G., F.S., S.P., and D.M.; supervision, F.S.

## DECLARATION OF INTERESTS

The authors declare no competing interests.

Received: December 20, 2022
Revised: February 10, 2023
Accepted: May 22, 2023
Published: June 12, 2023

## REFERENCES


1. Traverse, C.J., Pandey, R., Barr, M.C., and Lunt, R.R. (2017). Emergence of highly transparent photovoltaics for distributed applications. Nat. Energy *2*, 849–860. https://doi.org/10.1038/s41560-017-0016-9.

2. Lunt, R.R. (2012). Theoretical limits for visibly transparent photovoltaics. Appl. Phys. Lett. *101*, 043902. https://doi.org/10.1063/1.4738896.

3. Lunt, R.R., and Bulovic, V. (2011). Transparent, near-infrared organic photovoltaic solar cells for window and energy-scavenging applications. Appl. Phys. Lett. *98*, 113305. https://doi.org/10.1063/1.3567516.

4. Chen, C., Dou, L., Zhu, R., Chung, C., Song, T., Zheng, Y.B., and Al, C.E.T. (2012). Cells produced by solution processing. ACS Nano120712084458005.

5. Zhao, Y., Meek, G.A., Levine, B.G., and Lunt, R.R. (2014). Near-infrared harvesting transparent luminescent solar concentrators. Adv. Opt. Mater. *2*, 606–611. https://doi.org/10.1002/adom.201400103.

6. Zhang, K., Shi, Z.M., Chang, Y.N., Hu, Z.M., Qi, H.X., Hong, W., and Han, L. (2014). High-performance, transparent, dye-sensitized solar cells for see-through photovoltaic windows. Gene X. *547*, 1–9. https://doi.org/10.1002/aenm.201301966.

7. Roy, A., Ghosh, A., Bhandari, S., Selvaraj, P., Sundaram, S., and Mallick, T.K. (2019). Color comfort evaluation of dye-sensitized solar cell (DSSC) based building-integrated photovoltaic (BIPV) glazing after 2 Years of ambient exposure. J. Phys. Chem. C *123*, 23834–23837. https://doi.org/10.1021/acs.jpcc.9b05591.

8. Ghosh, A., Selvaraj, P., Sundaram, S., and Mallick, T.K. (2018). The colour rendering index and correlated colour temperature of dye-sensitized solar cell for adaptive glazing application. Sol. Energy *163*, 537–544. https://doi.org/10.1016/j.solener.2018.02.021.

9. Huaulmé, Q., Mwalukuku, V.M., Joly, D., Liotier, J., Kervella, Y., Maldivi, P., Narbey, S., Oswald, F., Riquelme, A.J., Anta, J.A., and Demadrille, R. (2020). Photochromic dye-sensitized solar cells with light-driven adjustable optical transmission and power conversion efficiency. Nat. Energy *5*, 468–477. https://doi.org/10.1038/s41560-020-0624-7.

10. Godfroy, M., Liotier, J., Mwalukuku, V.M., Joly, D., Huaulmé, Q., Cabau, L., Aumaitre, C., Kervella, Y., Narbey, S., Oswald, F., et al. (2021). Benzothiadiazole-based photosensitizers for efficient and stable dye-sensitized solar cells and 8.7% efficiency semi-transparent mini-modules. Sustain. Energy Fuels *5*, 144–153. https://doi.org/10.1039/D0SE01345E.

11. Vesce, L., Mariani, P., Calamante, M., Dessì, A., Mordini, A., Zani, L., and Di Carlo, A. (2022). Process engineering of semitransparent DSSC modules and panel incorporating an organic sensitizer. Sol. RRL *6*, 2200403–2200411. https://doi.org/10.1002/solr.202200403.

12. Ono, T., Yamaguchi, T., and Arakawa, H. (2009). Study on dye-sensitized solar cell using novel infrared dye. Sol. Energy Mater. Sol. Cells *93*, 831–835. https://doi.org/10.1016/j.solmat.2008.09.038.

13. Saccone, D., Galliano, S., Barbero, N., Quagliotto, P., Viscardi, G., and Barolo, C. (2016). Polymethine dyes in hybrid photovoltaics: structure-properties relationships. Eur. J. Org Chem. *2016*, 2244–2259. https://doi.org/10.1002/ejoc.201501598.

14. Naim, W., Novelli, V., Nikolinakos, I., Barbero, N., Dzeba, I., Grifoni, F., Ren, Y., Alnasser, T., Velardo, A., Borrelli, R., et al. (2021). Transparent and colorless dye-sensitized solar cells exceeding 75% average visible transmittance. JACS Au *1*, 409–426. https://doi.org/10.1021/jacsau.1c00045.

15. Cong, J., Yang, X., Hao, Y., Kloo, L., and Sun, L. (2012). A highly efficient colourless sulfur/iodide-based hybrid electrolyte for dye-sensitized solar cells. RSC Adv. *2*, 3625–3629. https://doi.org/10.1039/c2ra20310c.

16. Patel, M.U.M., Demir-Cakan, R., Morcrette, M., Tarascon, J.M., Gaberscek, M., and Dominko, R. (2013). Li-S battery analyzed by UV/vis in operando mode. ChemSusChem *6*, 1177–1181. https://doi.org/10.1002/cssc.201300142.

17. Barchasz, C., Molton, F., Duboc, C., Leprêtre, J.C., Patoux, S., and Alloin, F. (2012). Lithium/sulfur cell discharge mechanism: an original approach for intermediate species identification. Anal. Chem. *84*, 3973–3980. https://doi.org/10.1021/ac2032244.

18. Cañas, N.A., Fronczek, D.N., Wagner, N., Latz, A., and Friedrich, K.A. (2014). Experimental and theoretical analysis of products and reaction intermediates of lithium-sulfur batteries. J. Phys. Chem. C *118*, 12106–12114. https://doi.org/10.1021/jp5013208.

19. Lu, Y.C., He, Q., and Gasteiger, H.A. (2014). Probing the lithium-sulfur redox reactions: a rotating-ring disk electrode study. J. Phys. Chem. C *118*, 5733–5741. https://doi.org/10.1021/jp500382s.

20. Zhang, G., Peng, H., Zhao, C., Chen, X., Zhao, L., Li, P., Huang, J., and Zhang, Q. (2018). The radical pathway based on a lithium-metal-compatible high-dielectric electrolyte for lithium–sulfur batteries. Angew. Chem. *130*, 16974–16978. https://doi.org/10.1002/ange.201810132.

21. Zou, Q., Liang, Z., Du, G.Y., Liu, C.Y., Li, E.Y., and Lu, Y.C. (2018). Cation-directed selective polysulfide stabilization in alkali metal-sulfur batteries. J. Am. Chem. Soc. *140*, 10740–10748. https://doi.org/10.1021/jacs.8b04536.

22. He, Q., Gorlin, Y., Patel, M.U.M., Gasteiger, H.A., and Lu, Y.-C. (2018). Unraveling the correlation between solvent properties and sulfur redox behavior in lithium-sulfur batteries. J. Electrochem. Soc. *165*, A4027–A4033. https://doi.org/10.1149/2.0991816jes.

23. Boschloo, G., Gibson, E.A., and Hagfeldt, A. (2011). Photomodulated voltammetry of iodide/triiodide redox electrolytes and its relevance to dye-sensitized solar cells. J. Phys. Chem. Lett. *2*, 3016–3020. https://doi.org/10.1021/jz2014314.

24. Datta, J., Bhattacharya, A., and Kundu, K.K. (1988). Relative standard electrode potentials of I 3 −/I − , I 2/I 3 − , and I 2/I − redox couples and the related formation constants of I 3 − in some pure and mixed dipolar aprotic solvents. Bull. Chem. Soc. Jpn. *61*, 1735–1742. https://doi.org/10.1246/bcsj.61.1735.

25. Pydzińska, K., and Ziółek, M. (2015). Solar cells sensitized with near-infrared absorbing dye: problems with sunlight conversion efficiency revealed in ultrafast laser spectroscopy studies. Dyes Pigm. *122*, 272–279. https://doi.org/10.1016/j.dyepig.2015.07.003.

26. Bonomo, M., Saccone, D., Magistris, C., Barolo, C., Ciná, L., Carlo, A.D., and Dini, D. (2017). Influence of the conditions of sensitization on the characteristics of p -DSCs sensitized with asymmetric squaraines. J. Electrochem. Soc. *164*, H1099–H1111. https://doi.org/10.1149/2.0971714jes.

27. Chandiran, A.K., Zakeeruddin, S.M., Humphry-Baker, R., Nazeeruddin, M.K., Grätzel, M., and Sauvage, F. (2017). Investigation on the interface modification of TiO2 surfaces by functional Co-adsorbents for high-efficiency dye-sensitized solar cells. ChemPhysChem *18*, 2724–2731. https://doi.org/10.1002/cphc.201700486.

28. Buskens, P., Burghoorn, M., Mourad, M.C.D., and Vroon, Z. (2016). Antireflective coatings for glass and transparent polymers. Langmuir *32*, 6781–6793. https://doi.org/10.1021/acs.langmuir.6b00428.

29. Zhao, Y., and Lunt, R.R. (2013). Transparent luminescent solar concentrators for large-area solar windows enabled by massive Stokes-shift nanocluster phosphors. Adv. Energy Mater. *3*, 1143–1148. https://doi.org/10.1002/aenm.201300173.

30. Schubert, E.F. (2006). Light-Emitting Diodes (Cambridge University Press).

31. Williams, M.P.A., Ethirajan, M., Ohkubo, K., Chen, P., Pera, P., Morgan, J., White, W.H., Shibata, M., Fukuzumi, S., Kadish, K.M., and Pandey, R.K. (2011). Synthesis, photophysical, electrochemical, tumor-imaging, and phototherapeutic properties of purpurinimide-N-substituted cyanine dyes joined with variable lengths of linkers. Bioconjugate Chem. *22*, 2283–2295. https://doi.org/10.1021/bc200345p.

32. Li, D., Li, H., Luo, Y., Li, K., Meng, Q., Armand, M., and Chen, L. (2010). Non-corrosive, non-absorbing organic redox couple for dye-sensitized solar cells. Adv. Funct. Mater. *20*, 3358–3365. https://doi.org/10.1002/adfm.201000150.

33. Rowley, J.G., Ardo, S., Sun, Y., Castellano, F.N., and Meyer, G.J. (2011). Charge recombination to oxidized iodide in dye-sensitized solar cells. J. Phys. Chem. C *115*, 20316–20325. https://doi.org/10.1021/jp204675p.